


## Article

# Analysis of Sealing Performance of Metal B-ring Self-Tightening Structure

Bingjun Gao <sup>1,\*</sup> , Han Gao <sup>1</sup>, Junhua Dong <sup>1,\*</sup>, Yongming An <sup>2,\*</sup> and Chuanzhi Wang <sup>3</sup>

<sup>1</sup> School of Chemical Engineering and Technology, Hebei University of Technology, Tianjin 300130, China; 201921502014@stu.hebut.edu.cn

<sup>2</sup> SINOPEC Beijing Yanshan Company, Beijing 102500, China

<sup>3</sup> Beijing Yanhua Engineering Construction Company, Beijing 102502, China; wangcz@byce.cn

\* Correspondence: bjgao@hebut.edu.cn (B.G.); djh2006@hebut.edu.cn (J.D.); anym.yssh@sinopec.com (Y.A.)

**Abstract:** Process industries often use B-ring self-tightening sealing structures and rely on interference assembly to meet the initial sealing requirements. Therefore, determining reasonable B-ring material, size and interference is crucial to ensure the sealing performance of the structure. In this paper, based on elastic deformation analysis, the deformation co-ordination equation of a B-ring sealing structure was established, and a sealing contact pressure calculation formula was obtained, with discussion of the main factors affecting sealing performance. With the finite element method, transient temperature field analysis was carried out for startup and shutdown load cases, and contact analysis was carried out for interference assembly, startup and shutdown. Based on the evaluation criteria of sealing performance with proposed sealing rate and leakage parameters, the effects of material properties, interference, B-ring size, etc., on sealing performance were investigated, revealing that although a B-ring with high material yield stress can meet the sealing requirements, both the B-ring and the sealing surface of a reactor body will yield plastic deformation. B-rings with a low material yield stress exhibit obvious plastic deformation during startup and leak during shutdown. However, leakage parameters can be minimized by smaller interference and moderate wave radius.



**Citation:** Gao, B.; Gao, H.; Dong, J.; An, Y.; Wang, C. Analysis of Sealing Performance of Metal B-ring Self-Tightening Structure. *Processes* **2022**, *10*, 1084. <https://doi.org/10.3390/pr10061084>

Academic Editor: Chi-Min Shu

Received: 23 April 2022

Accepted: 25 May 2022

Published: 29 May 2022

**Publisher's Note:** MDPI stays neutral with regard to jurisdictional claims in published maps and institutional affiliations.



**Copyright:** © 2022 by the authors. Licensee MDPI, Basel, Switzerland. This article is an open access article distributed under the terms and conditions of the Creative Commons Attribution (CC BY) license (<https://creativecommons.org/licenses/by/4.0/>).

**Keywords:** B-ring; self-tightening seal; FEM; leakage

## 1. Introduction

In high-pressure vessels and pipeline connection structures, the B-ring seal is a kind of radial self-tightening structure [1] with a good sealing effect in a large-diameter seal structure. When the effective contact pressure of a sealing surface is a multiple of medium pressure [2] or yield stress [3], the effective sealing of the equipment can be guaranteed. B rings have two forms: composite B rings and the metal B rings. A composite B-ring is generally composed of a metal body, two nonmetallic gaskets and two metal clamp rings, in which the nonmetal gasket is susceptible to high-temperature aging and reduces the sealing performance of the B ring [4]. A metal B ring is a complete metal ring with two wave surfaces.

Although B-ring self-tightening seals have been used in industry for many years [5], the reasonable size, material and assembly size are considerably influenced by the connecting structure and operating conditions [6], so a design standard has not been established. Limited research has been conducted on self-sealing [7–9], with even fewer studies on B rings. Gao et al. [4] studied the effects of high-temperature aging, creep, system temperature and pressure, assembly size and other factors on the sealing performance of a combined B ring. Ryś et al. [10–12] conducted detailed theoretical research on metal B rings under preload and pressurization conditions. Trojnacki equated a B-ring to a shell model with equal thickness simply supported at both ends of the surface. Through finite element analysis based on shell theory, several calculation models of an all-metal B ring under pressure were studied [13], and the influences of several parameters on the strength

and sealing performance of B rings were determined [14–16]. On this basis, the fitting and sealing surface flatness were limited [17]. However, these results are more conservative, and the influence of temperature was not taken into account.

According to the survey, it is found that the metal B-ring seals used in high-pressure reactors often leak when pressure is reduced, which affects the safe operation of factories. High-temperature and high-pressure production conditions, material performance and the structure size of the B ring have an impact on B-ring sealing performance. Therefore, in this paper, with consideration of temperature, pressure, structure size and material performance, we analyzed the failure cause of a sealing structure through deformation co-ordination analysis in the elastic range; furthermore, through finite element calculation of startup and shutdown, we determined reasonable metal material and B-ring size to ensure reliable sealing.

## 2. B-ring Sealing Mechanism, Working Condition Analysis and Material Properties of High-Pressure Reactors

The B-ring sealing structure of a high-pressure reactor is shown in Figure 1, which consist of a cylinder, clamp, end cover, nozzle and B ring. The B ring adopts interference fit with the sealing surfaces of the cylinder and end cover. The clamp adopts a 1/2 split structure. There is a 1/2 split hollow jacket outside the cylinder for heat exchange, with water cooling during normal operation and steam heating or heat preservation at the end of startup and shutdown.

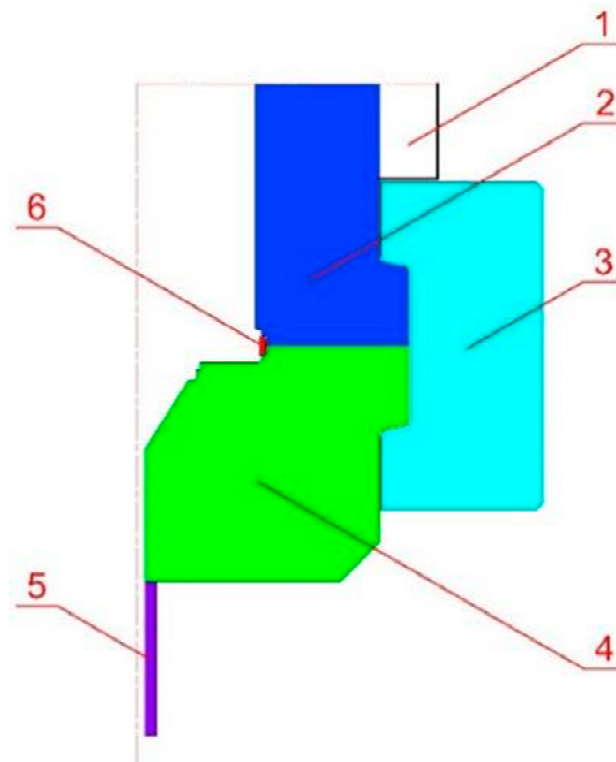


**Figure 1.** B-ring sealing structure of a high-pressure reactor. 1, jacket; 2, cylinder; 3, clamp; 4, end cover; 5, nozzle; 6, B ring.

The reactor is in a heat-preservation state before startup, and steam is introduced into the hollow jacket to keep it warm. The temperature of the outer wall of the reactor is 150 °C at all times. The temperature–pressure curve in the working conditions of startup and shutdown is shown in Figure 2. Startup condition and shutdown condition are divided into three stages according to changes in pressure and temperature.

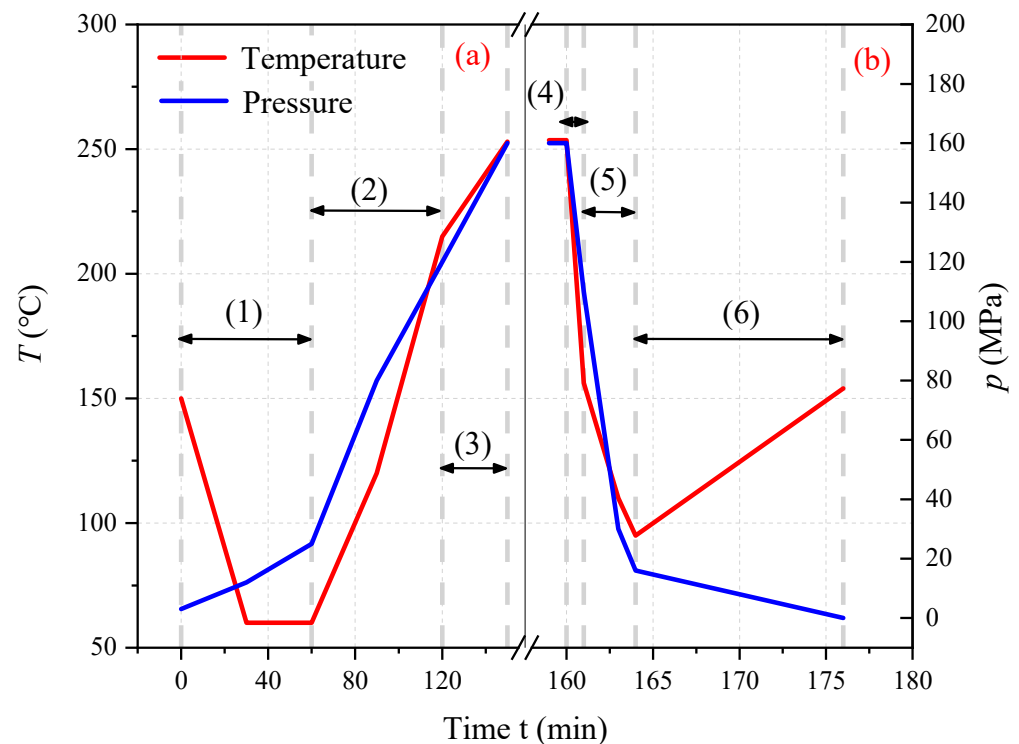


**Figure 2.** Temperature–pressure curve in real time: (a) heating and pressure increase condition; (b) cooling and depressurization condition.

Stages (1)–(3) include heating and pressurization; pressure increases with the continuous filling of cold materials. A catalyst is added at the end of stage (1) to initiate an exothermic reaction in the reactor, and the temperature begins to rise. At the end of stage (2), the jacket is fed with cold water to cool reactor body, and the reaction in the reactor continues. At the end of stage (3), the pressure and temperature remain stable, and the reactor enters the normal production condition.

Stages (4)–(6) comprise shutdown, cooling and depressurization. Temperature and pressure drop rapidly in stages (4) and (5). In stage (6), nitrogen is introduced to discharge partially or completely unreacted materials in the reactor, and steam is introduced into the hollow jacket to increase the temperature and slowly reduce the pressure.

The design conditions of the reactor are shown in Table 1, in which several B-ring materials are also presented for discussion and analysis. Material properties required for temperature field and stress field analysis of a reactor B-ring seal structure [18] are shown in Figure 3. In addition, Poisson's ratio of materials is 0.3, and the density is 7750 kg/m<sup>3</sup>.

**Table 1.** Design conditions of a reactor.

Name	Parameters
Operating temperature/(°C)	253
Work pressure/(MPa)	160
Design temperature/(°C)	300
Design pressure/(MPa)	260
Hydrostatic test pressure/(MPa)	332
Cylinder, clamp, end cover and nozzle material	NiCrMoV
Proposed B-ring material	10/20/16 Mn/NiCrMoV/4140
Cylinder radius/(mm)	229.616
Cylinder contact surface radius, $R_{c1}$ /(mm)	250.830
Clamp outer radius, $R_{c2}$ /(mm)	787.400

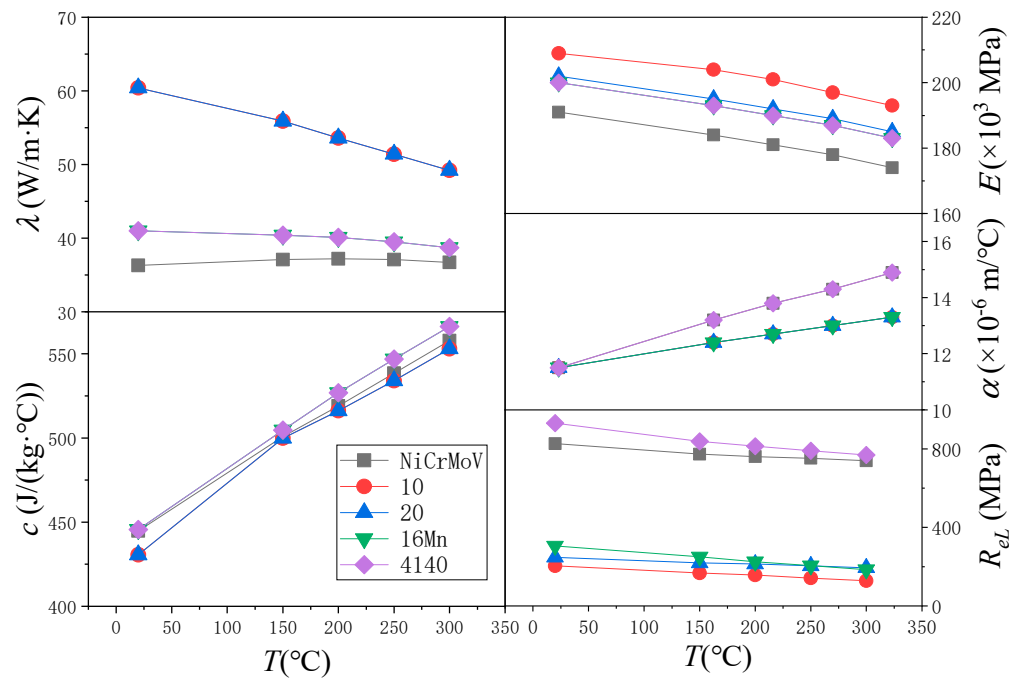


Figure 3. Material properties.

### 3. Evaluation Criteria of Sealing Performance

The sealing performance of the structure is usually evaluated according to the average contact pressure within the effective width range. One view is that the average contact pressure is greater than the yield stress of material to meet the sealing requirements [14–16], namely:

$$Q > n\sigma_s^t \quad (1)$$

where  $Q$  is the average contact pressure within the effective contact pressure range of the gasket;  $\sigma_s^t$  is the yield stress of the gasket material at room temperature or design temperature; and  $n$  is the shim coefficient, which is 1.5 when preloading and 1.0 when working.

This evaluation method was proposed for a lens-shaped ring sealing structure, which is essentially a forced with a certain self-tightening sealing effect.

Another evaluation method was proposed for the sealing structure of a metal ring gasket, considering that the sealing can be realized as long as the average contact pressure of the gasket within the effective contact width is  $m$  times the medium pressure [19] in the operating state, namely:

$$Q > mp \quad (2)$$

where  $p$  is the medium pressure; and  $m$  is the shim coefficient:  $m = 5.5$  for mild steel,  $m = 6.0$  for Monel or 4%~6% chrome steel and  $m = 6.5$  for stainless steel.

Metal ring sealing is essentially a radial self-tightening structure, which is closer to the B-ring sealing structure.

Combining the two evaluation methods of sealing performance, the following evaluation methods were used to evaluate the sealing performance of a B-ring sealing structure:

(1) When the effective contact pressure,  $Q$ , of the sealing surface is less than the yield stress,  $\sigma_s^T$ , of the material at  $T$  °C, use (2) to evaluate.

(2) When the effective contact pressure,  $Q$ , of the sealing surface is greater than the yield stress,  $\sigma_s^T$ , of the material at  $T$  °C:

$$Q > \sigma_s^T \quad (3)$$

The sealing ratio was defined as the ratio of  $Q$  to  $mp$  (or  $\sigma_s^T$ ). When the sealing ratio is less than 1, the sealing is expected to fail, causing the reactor to leak. When the medium

pressure,  $p$ , is 0 MPa, to facilitate the calculation of the sealing rate, the medium pressure,  $p$ , is regarded as 1 MPa.

#### 4. Analysis of B-ring Seal Structure Based on Elastic Deformation

According to the strength condition, the thickness of the B ring was determined on the basis of the design pressure and hydrostatic test pressure; then, the inner and outer diameters of the B ring were calculated. Finally, the average contact pressure and contact width between the B ring, cylinder and end cover were calculated in the elastic range according to the deformation caused by temperature load and pressure load, respectively, as well as the deformation co-ordination relationship.

##### 4.1. Determination of B-ring Thickness

A schematic diagram of partial dimensions of the B-ring seal structure is shown in Figure 4.

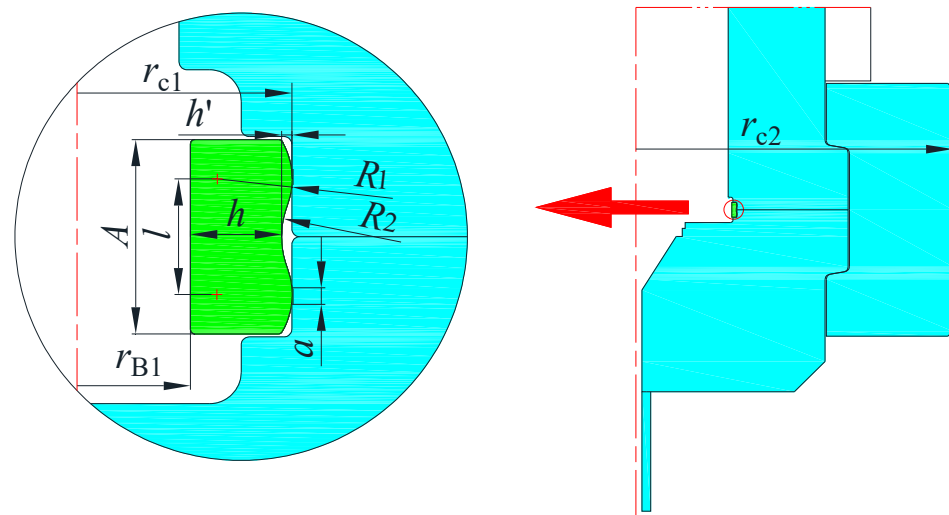


**Figure 4.** B-ring dimensions.

The maximum bending normal stress,  $\sigma_T$ , in the middle of the B ring under hydraulic test conditions should meet the following requirements:

$$\sigma_T = \frac{3p_T(l-a)^2}{4h_1^2} \leq 0.9R_{el}^0 \quad (4)$$

where  $p_T$  is the hydraulic test pressure;  $R_{el}^0$  is the yield stress of the B-ring material at room temperature;  $l$ , related to the reactor cylinder radius, is 22.2 mm; and the contact width,  $a$ , is mainly related to the yield stress of materials. The values of different B-ring materials are shown in Table 2.

**Table 2.** Maximum contact width and minimum thickness of B rings of different materials.

Material	10	20	16 Mn	NiCrMoV	4140
$a$ /(mm)	7.0	5.5	5.5	2.0	2.0
$h$ /(mm)	17.7	17.6	15.9	11.7	11.0

According to the yield stress of selected materials, the minimum thickness,  $h_1$ , of the B ring that meet the strength requirements of the hydrostatic test can be obtained.

Under the design conditions, the maximum bending normal stress,  $\sigma$ , in the middle of the B ring should meet the following requirements:

$$\sigma = \frac{3p(l-a)^2}{4h_2^2} \leq 1.5[\sigma]^t \quad (5)$$

Therefore, the minimum thickness of the B ring can be determined as follows:

$$h = \max[h_1, h_2] \quad (6)$$

The minimum thickness of B rings for different materials are also shown in Table 2. The wave height of the B ring can be calculated according to its the structural characteristics:

$$h' = R_1 + R_2 - \sqrt{R_1^2 - \left[ \frac{R_1 \cdot l}{2(R_1 + R_2)} \right]^2} - \sqrt{R_2^2 - \left[ \frac{R_2 \cdot l}{2(R_1 + R_2)} \right]^2} \quad (7)$$

The width of the B ring can be determined as follows:

$$A = l + 2\sqrt{2R_1h' - h'^2} \quad (8)$$

The average thickness of the B ring is expressed as follows:

$$\bar{h} = \frac{S_B}{A} \quad (9)$$

where  $S_B$  is the cross-sectional area of the B ring ( $\text{mm}^2$ ).

The equivalent outer radius of the B ring is proposed as follows:

$$r_{B2} = D_{B1}/2 + \bar{h} = r_{B1} + \bar{h} \quad (10)$$

#### 4.2. Calculation of the Contact Pressure

The contact pressure between the B-ring sealing structure of the reactor and the sealing surface is affected by the B-ring initial interference, temperature and pressure. When the contact pressure is relatively low, the B ring only produces elastic deformation, and when the contact pressure is greater than the yield stress of the B-ring material, the contact surfaces of the B ring will produce plastic deformation. Similarly, when the contact pressure is greater than the yield stress of the cylinder and the end-cover material, plastic deformation will also occur in the relative positions of the contact surfaces. In the following paragraphs, only the elastic deformation stage of the cylinder and the B-ring was analyzed.

As shown in Figure 5, the radial displacement of the B-ring is  $\Delta_B^P$  under medium pressure,  $\Delta_B^T$  under temperature, and  $\Delta_B^Q$  under contact pressure.  $\Delta_B^P, \Delta_B^T$  and  $\Delta_B^Q$  are the deformations in the equivalent radius of the B ring. The cylinder is only subject to the contact pressure in the contact area with the B ring but is still affected by the medium pressure outside the contact area. When only the cylinder displacement caused by the medium pressure is discussed, the radial displacement caused by the contact pressure transmitted to the cylinder through the B ring is obviously less than that directly caused by medium pressure. Therefore, the radial displacement of the cylinder calculated for medium pressure is larger, and the contact pressure between the cylinder and the B ring is lower. For the sake of conservativeness, the radial displacement of the cylinder is approximately that generated directly the medium pressure, that is,  $\Delta_c^{P+Q} = \Delta_c^P$ . The radial displacement of the cylinder caused by temperature is  $\Delta_c^T$ , and  $\Delta_c^{P+Q}$  and  $\Delta_c^T$  are the deformation at the sealing surface of the cylinder. The end of the cylinder and the clamp are in contact with each other, and they are not separated during the assembly and pressure-bearing process. Therefore, the calculated outer radius of the cylinder is approximately equal to the outer radius of the clamp,  $r_{c2}$ .

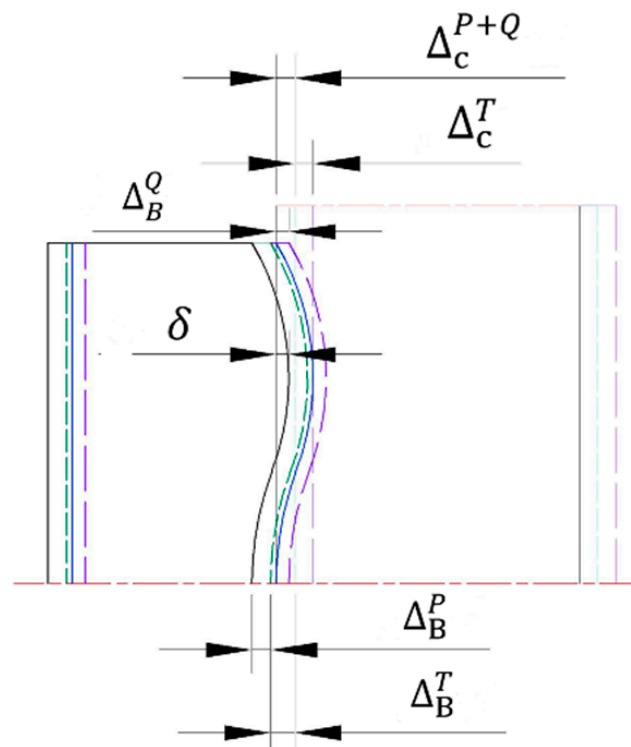


**Figure 5.** Schematic diagram of deformation co-ordination.

Deformation co-ordination between the B ring and cylinder is expressed as:

$$\left[ \Delta_B^P + \Delta_B^T + \delta - \Delta_B^Q \right] - \left[ \Delta_c^{P+Q} + \Delta_c^T \right] = 0 \quad (11)$$

To obtain the contact pressure,  $Q$ , it is necessary to provide the deformation of the B ring and cylinder under temperature and pressure.

#### 4.2.1. Radial Deformation by Temperature Load

For a cylinder with an initial temperature,  $T_0$ ; inner radius,  $r_1$ ; outer radius,  $r_2$ ; inner wall temperature,  $T_1$ ; and outer wall temperature,  $T_2$ , the thermal deformation [20] can be divided into free deformation by temperature and thermal deformation by thermal stress.

Free thermal deformation is expressed as:

$$\Delta_r = r \cdot \alpha \frac{(T_1 - T_0) \ln \frac{r_2}{r} + (T_2 - T_0) \left( \ln \frac{r_2}{r_1} - \ln \frac{r_2}{r} \right)}{\ln \frac{r_2}{r_1}} \quad (12)$$

The deformation caused by thermal stress is expressed as:

$$u_r = r \cdot \frac{\alpha(T_1 - T_2)}{2(1 - \mu)} \left[ \frac{1 - \ln \frac{r_2}{r}}{\ln \frac{r_2}{r_1}} - \frac{r_1}{r} - \mu \left( \frac{1 - 3 \ln \frac{r_2}{r}}{\ln \frac{r_2}{r_1}} - \frac{\left( \frac{r_2}{r} \right)^2 - 3}{\left( \frac{r_2}{r_1} \right)^2 - 1} \right) \right] \quad (13)$$

The total deformation caused by temperature load is expressed as:

$$\Delta^T = \Delta_r + u_r \quad (14)$$

For the B ring, the uniform temperature is  $T$ ; and  $r_1$  and  $r_2$  are  $r_{B1}$  and  $r_{B2}$ , respectively. The deformation by temperature load at  $r_{B2}$  is expressed as:

$$\Delta_B^T = \Delta_{Br} = r_{B2} \alpha_B (T - T_0) \quad (15)$$

For the cylinder,  $r_1$  and  $r_2$  are  $r_{c1}$  and  $r_{c2}$ , respectively; and the inner and outer wall temperatures are  $T_{c1}$  and  $T_{c2}$ , respectively. The deformation by temperature load at  $r_{c1}$  is expressed as:

$$\Delta_c^T = r_{c1} \left\{ \frac{\alpha_c(T_1 - T_2)}{2(1 - \mu_c)} \left[ \frac{1}{\ln \frac{r_{c2}}{r_{c1}}} - 2 - \mu_c \left( \frac{1 - 3 \ln \frac{r_{c2}}{r_{c1}}}{\ln \frac{r_{c2}}{r_{c1}}} - \frac{\left(\frac{r_{c2}}{r_{c1}}\right)^2 - 3}{\left(\frac{r_{c2}}{r_{c1}}\right)^2 - 1} \right) \right] + \alpha_c(T_{c1} - T_{c0}) \right\} \quad (16)$$

#### 4.2.2. Deformation by Pressure Load

For a thick-walled cylinder with an inner radius,  $r_1$ ; outer radius,  $r_2$ ; and inner wall pressure,  $p$ , radial displacement at radius  $r$  under closed conditions is expressed as:

$$\Delta = \frac{r}{E(r_2^2 - r_1^2)} \left[ (1 - 2\mu)pr_1^2 + (1 + \mu)\frac{pr_1^2r_2^2}{r^2} \right] \quad (17)$$

The radial displacement at radius  $r$  under opening condition is expressed as:

$$\Delta = \frac{r}{E(r_2^2 - r_1^2)} \left[ (1 - \mu)pr_1^2 + (1 + \mu)\frac{pr_2^2}{r^2} \right] \quad (18)$$

For B rings, which can be regarded as openings, the deformation caused by the pressure load is expressed as:

$$\Delta_B^P = \frac{2pr_{B1}^2r_{B2}}{E_B^T(r_{B2}^2 - r_{B1}^2)} \quad (19)$$

For a cylinder, which can be regarded as a closed mouth, the deformation caused by pressure load is expressed as:

$$\Delta_c^{P+Q} = \frac{r_{c1}p}{E_c^T(r_{c2}^2 - r_{c1}^2)} \left[ (1 - 2\mu_c)r_{c1}^2 + (1 + \mu_c)r_{c2}^2 \right] \quad (20)$$

#### 4.2.3. Deformation by Contact Pressure

The radial deformation of a cylinder caused by contact pressure of the B ring can be conservatively calculated with Equation (21). Only the radial displacement of the B ring under contact pressure is considered here.

Under the contact pressure,  $Q$ , of the ring, the relationship between  $Q$  and the hoop strain,  $\varepsilon_\theta$ , of the B ring can be approximately expressed as:

$$2Qar_{B2} = E_B^T\varepsilon_\theta(r_{B2} - r_{B1})A \quad (21)$$

The deformation of the B ring due to contact pressure is expressed as:

$$\Delta_B^Q = \varepsilon_\theta r_{B2} = \frac{2Q \cdot r_{B2}^2}{E_B^T(r_{B2} - r_{B1})} \cdot \frac{a}{A} \quad (22)$$

where, according to Hertz's theory, the arc surface contact width [21] is:

$$a = \frac{8QR_1}{\pi} \cdot \left( \frac{1 - \mu_B^2}{E_B^T} + \frac{1 - \mu_c^2}{E_c^T} \right) \quad (23)$$

Substitute (24) into Equation (23) to obtain:

$$\Delta_B^Q = \frac{16Q^2 \cdot r_{B2}^2}{E_B^T(r_{B2} - r_{B1})} \cdot \frac{R_1}{\pi A} \cdot \left( \frac{1 - \mu_B^2}{E_B^T} + \frac{1 - \mu_c^2}{E_c^T} \right) \quad (24)$$

where  $\mu_B = \mu_c = 0.3$ .



#### 4.2.4. Analysis of Contact Pressure

The effective contact pressure of the B ring is obtained by inputting Equations (15), (16), (19), (20) and (24) into the deformation co-ordination Equation (12):

$$Q = \sqrt{\frac{\pi E_B^T A \cdot (r_{B2} - r_{B1})}{16 R_1 r_{B2}^2 (1 - \mu^2)} \cdot \frac{E_B^T \cdot E_c^T}{E_B^T + E_c^T} \cdot \left\{ \left[ \Delta_B^p + \Delta_B^T + \delta \right] - \left[ \Delta_c^{p+Q} + \Delta_c^T \right] \right\}} \quad (25)$$

It can be seen from Equation (25) that within the elastic range of the same material of the B ring, the parameters that can affect the average contact pressure,  $Q$ , are as follows: temperature,  $T$ ; pressure,  $p$ ; allowable stress of B-ring material; yield stress; elastic modulus,  $E_B$ ; linear expansion coefficient,  $\alpha_B$ , of the B ring; elastic modulus,  $E_c$  and linear expansion coefficient,  $\alpha_c$ , of the cylinder material; cylinder inner diameter,  $r_{c1}$ , and outer diameter  $r_{c2}$ ; B-ring arc radius  $R_1$ ,  $R_2$ ; and the interference,  $\delta$ .

Because 10, 20 and 16 Mn steels produce plastic deformation in the assembly stage, only a B-ring made of 4140 steel was analyzed herein. Considering that the arc radius,  $R_2$ , of the B ring has little effect on its equivalent outer radius,  $r_{B2}$ ,  $R_2$  was fixed at 17.5 mm. Here, the influence of radius,  $R_1$ ; interference,  $\delta$ ; temperature,  $T$ ; and medium pressure,  $p$ , of the B ring on contact pressure and contact width are discussed.

According to the results of finite element simulation, three working points of the B-ring seal structure in a completely elastic state, namely, assembly working conditions, 0 min and 60 min working conditions (listed in Table 3), were selected for analysis and calculation. The temperatures of the cylinder and B ring were obtained by finite element simulation.

**Table 3.** Temperature at different positions under different conditions (°C)<sup>1</sup>.

Location	Assembly Condition (0 MPa)		0 min (0 MPa)		60 min (25 MPa)	
	$T_1$	$T_2$	$T_1$	$T_2$	$T_1$	$T_2$
B ring		20.0		70.0		61.0
Cylinder	20.0	20.0	70.0	35.0	63.5	40.00

<sup>1</sup>  $T_1$  is the inner wall temperature;  $T_2$  is the outer wall temperature. The initial temperature,  $T_0$ , is 20 °C.

The changes in the average contact pressure,  $Q$ , and the contact width,  $a$ , of a B ring with an arc radius,  $R_1$ , and interference,  $\delta$ , at different times and under different working conditions are shown in Figure 6. It can be seen that there is a higher-than-average contact pressure,  $Q$ , with a smaller arc radius,  $R_1$ , and a larger interference,  $\delta$ . A larger arc radius,  $R_1$ , and larger interference,  $\delta$ , can lead to a larger the contact width,  $a$ . Under different structural parameters,  $Q$  and  $a$  increase with  $T$  and  $p$ .

Although Equations (23) and (25) can be used to calculate the effective contact pressure,  $Q$ , and contact width,  $a$ , of the B ring in the elastic stage under different conditions, the plastic deformation of the B ring is inevitable during the operation cycle, especially when a material with lower yield stress is used. At this time, the effective contact pressure,  $Q$ , and contact width,  $a$ , of the B ring can be calculated by finite element simulation.

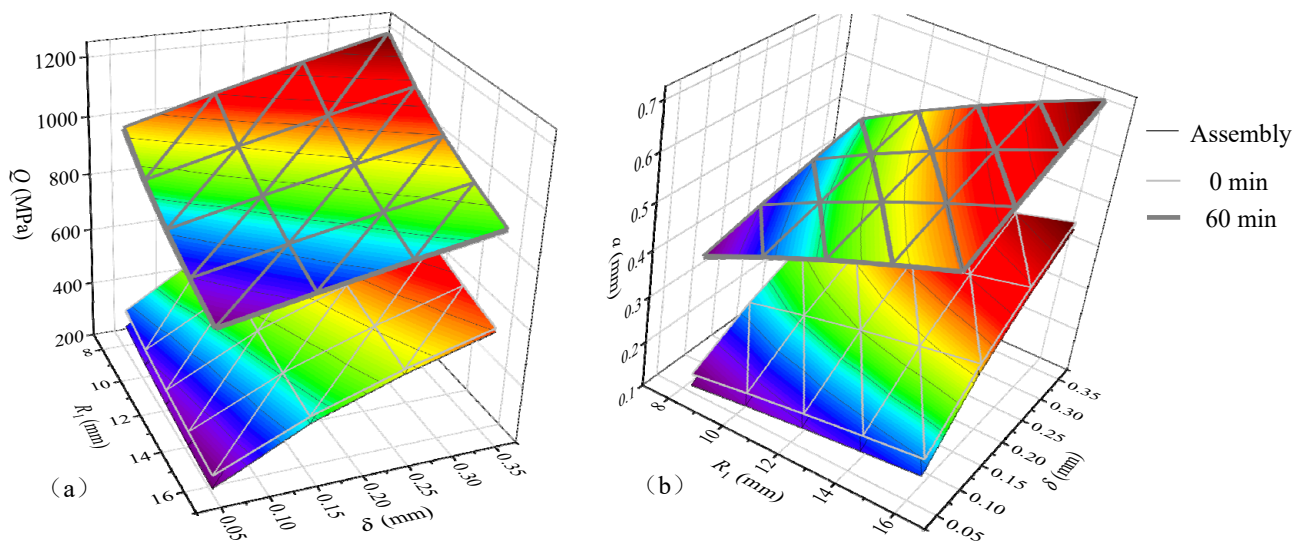


**Figure 6.** The influence of arc radius,  $R_1$ , and interference,  $\delta$ , on average contact pressure,  $Q$ , and contact width,  $a$ . (a) Average contact pressure,  $Q$ ; (b) contact width,  $a$ .

## 5. Finite Element Analysis

To obtain the sealing effect of the B-ring seal structure in different stages of the process, a finite element analysis model is established. First, assuming a 20 steel B-ring with an arc radius,  $R_1$ , of 14.3 mm; an inner arc radius,  $R_2$ , of 17.5 mm; and an interference,  $\delta$ , of 0.15 mm as an example, the transient temperature field of the structure was analyzed. Then, the calculated temperature load was applied to the structure, together with the pressure, and the average contact pressure of the B ring was obtained through contact analysis; then, the sealing performance was evaluated.

To investigate the influence of various factors on the sealing performance of the B ring, the material properties and crucial structural dimensions of the B ring were parametrically calculated and analyzed.

### 5.1. Finite Element Model and Boundary Conditions

#### 5.1.1. Finite Element Models and Simplification

According to the sealing structure and load characteristics of the reactor, an axisymmetric model was used. The model includes part of the cylinder and its end, the end cover (including its nozzle), the clamp and the B ring. Because the rigidity of the 1/2 split hollow jacket outside the cylinder is much lower than that of the cylinder, the hollow jacket was ignored in the model, and its heating effect on the cylinder was replaced by equivalent convective heat transfer. 2D solid elements were used to mesh the structure. The division of grid is shown in Figure 7. The thermal analysis used the Plane55 element, and the structural analysis used the Plane182 element. There were five contact pairs in the model, namely the contact between the end of the cylinder, the end cover and the clamp; the contact between the B-ring and sealing surfaces of the cylinder and the end cover; and the contact between the cylinder and the end cover. For the contact calculation, we used the target unit, Target169, and the contact unit, Conta172.

#### 5.1.2. Boundary Conditions

##### Calculation of Heat Transfer Boundary Conditions in the Transient Temperature Field

The upper-end face of the cylinder and the end face of the nozzle are thermal insulation boundaries. The convective heat transfer boundaries include the medium contact parts of the cylinder body and its end, the end cover and its nozzle, and the B ring. It also includes the air contact parts of the outside of the clamp. Considering the heat transfer effect of the hollow jacket outside the cylinder, the outer wall of the cylinder was set as the equivalent

convective heat transfer boundary. The contact thermal conductivity between the cylinder, the end cover, the clamp and the B ring was set to 3/2 of the thermal conductivity of the material. There was radiation heat transfer between the clamp, the cylinder and the end cover, and the emissivity coefficient was 0.75.

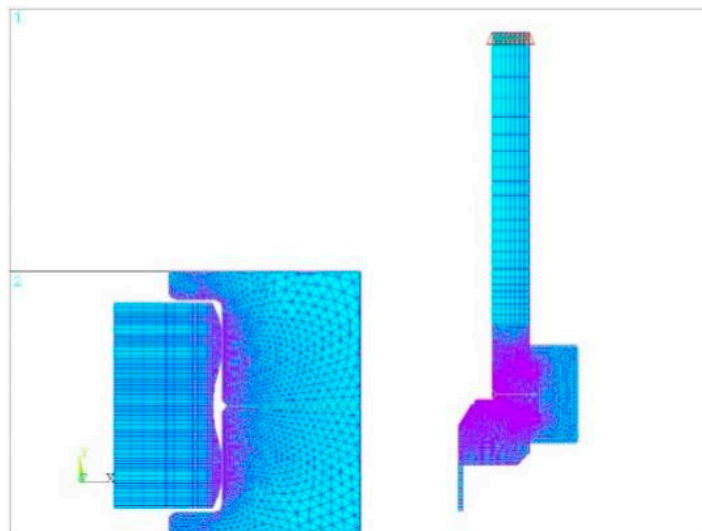


**Figure 7.** Mesh generation and constraint settings.

The reactor has three working conditions: heating up and boosting, normal operation, and cooling down and depressurizing. Among them, the two states of startup and shutdown are the most prone to reactor leakage. Therefore, the sealing of the reactor under these two working conditions were mainly simulated. According to the conditions, the convective heat transfer coefficient of heat transfer boundaries can be calculated through the empirical formula [22]; the heat transfer boundaries are shown in Table 4.

**Table 4.** Thermal analysis boundaries.

Working Conditions	Convective Heat Transfer Coefficient/W/(m <sup>2</sup> ·K)		Temperature of the Medium/°C		
	Inside the Reactor	Outside the Reactor with Jacket	Inside of Reactor	Inside the Jacket	Air
Normal operation	15,009	52.429	253.15	24	
Open or shutdown	13,135	116.282	186.575	142.04	0
Steam hold	10,384	81.997	150	250	

#### Boundaries for Structural Analysis

An axial displacement constraint was imposed on the upper-end face of the cylinder (as shown in Figure 7). Medium pressure was evenly applied to the inner wall of the B ring, the reactor, the end cover and the nozzle. At the same time, the end load was calculated according to Equation (27) and applied to the end of the nozzle.

$$p_c = \frac{p}{K^2 - 1} \quad (26)$$

where  $K$  is the diameter ratio of the nozzle, and  $p$  is the medium pressure (MPa).

Setting 20 °C as reference temperature at zero stress, stress–strain analysis of the structure was conducted by reading the node temperatures calculated by the transient thermal analysis as the temperature load and taking the medium pressure at the corresponding time as the mechanical load. The structural displacement field, stress–strain field and the contact pressure between the B ring and the sealing surface were obtained.

### 5.1.3. Mesh Independence Verification

The arc  $R_1$  of the B ring and the contact parts of the cylinder and the end cover were divided into 20, 40, 80, 100, and 120 divisions, respectively, and other parts were divided adaptively. Figure 8 shows the average contact pressure–pressure change curve on the cylinder side of the B ring under different fractions. In the process of heating and pressurization, the average contact pressure–pressure curve of the B-ring arc at 20 and 40 divisions was quite different from the other three curves. In the process of cooling and decompression, the overall coincidence of the five contact pressures is high, but the split curves of 20 and 80 divisions fluctuate considerably at about 25 MPa. Therefore, the 100 divisions of the B-ring arc surface can meet the requirements of mesh independence.

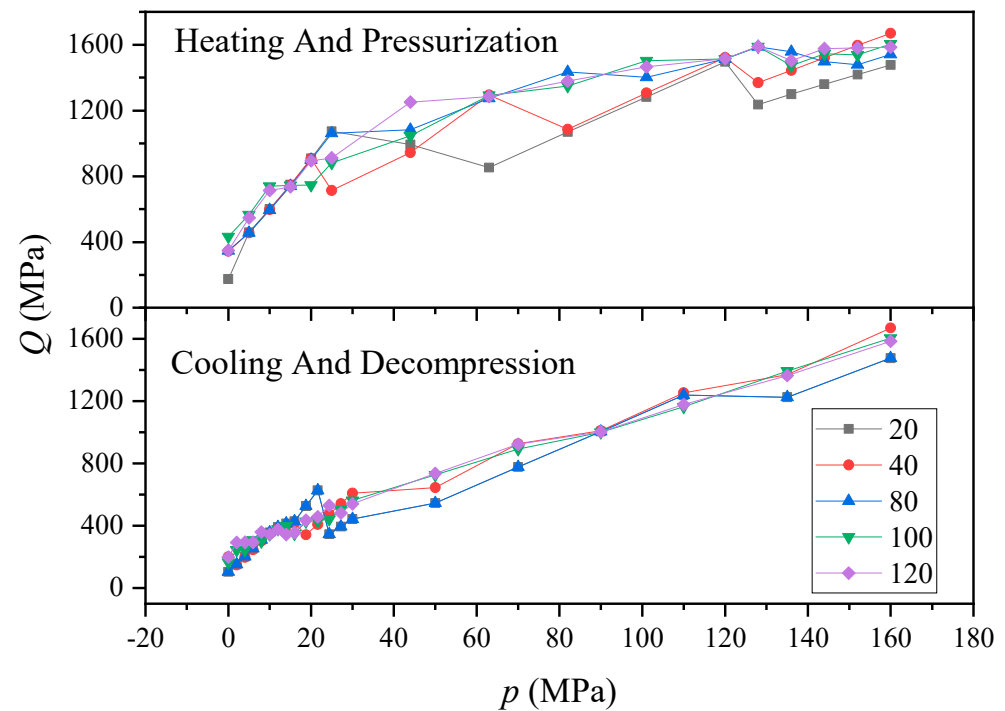


**Figure 8.** Contact pressure–pressure curves under different divisions.

## 5.2. An Example of Analysis

Assuming a 20 steel B ring with an arc radius,  $R_1$ , of 14.3 mm; an inner arc radius,  $R_2$ , of 17.5 mm; and an interference of 0.15 mm as an example, the calculation results of each working condition were obtained, and the leakage analysis was elucidated.

### 5.2.1. Calculation Results of Preloading Condition

The contact pressure contour of the sealing structure under preloading conditions is shown in Figure 9a, and the contact pressure distribution curves of the B-ring contact area on the cylinder side and the end-cover side is shown in Figure 9b. The area where the contact pressure is greater than 0 is defined as the effective contact area, and the contact pressure in the effective contact area can be calculated by Equation (27).

$$Q = \frac{\sum_1^n p_i \cdot (y_{i-1} - y_{i+1})}{2(y_1 - y_n) + y_1 - y_0 + y_{n+1} - y_n} \quad (27)$$

The average contact pressure on the cylinder side is 327.687 MPa, and that on the end-cover side is 329.308 MPa, which shows that the average contact pressure on the end-cover side is slightly higher than that on the cylinder side.

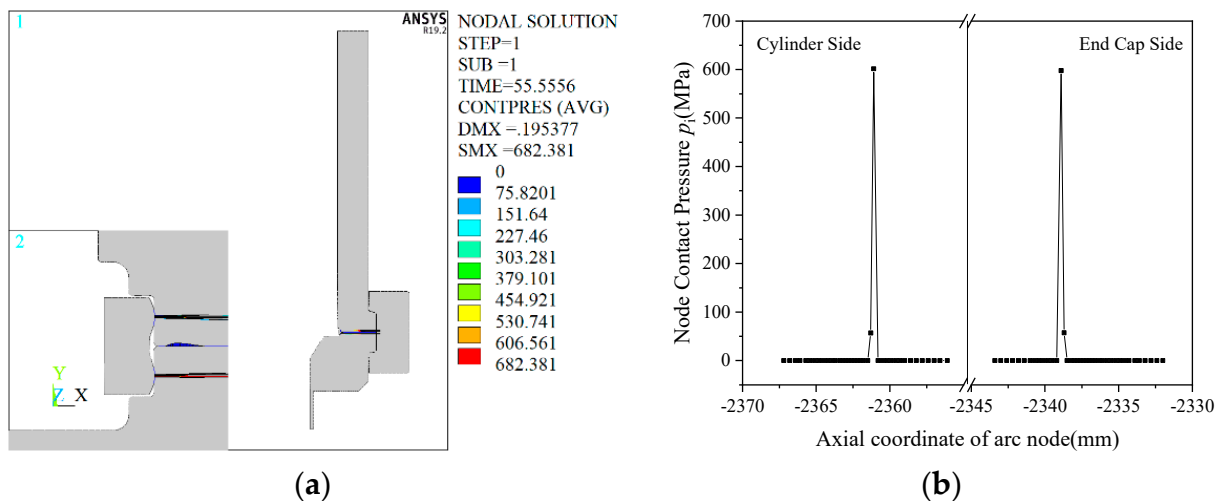


**Figure 9.** Contact pressure in preloading condition. (a) Contact pressure contour; (b) contact pressure distribution curve.

### 5.2.2. Calculation Result of the Process of Heating and Pressurization

The temperature contours, the contact pressure contours and the plastic deformation contours at different times during the heating and pressurization stage of the reactor are shown in Figure 10.

During the process of heating and pressurization, the medium pressure of the reactor increases continuously, and the contact pressure between the B ring and the cylinder, as well as the end cover, also increases due to the self-tightening. The maximum plastic strain near the contact area of the B ring also increases continuously. The average contact pressure and the maximum plastic strain of the cylinder side and the end-cover side in the process of heating and pressurization are shown in Figure 11. When the medium pressure is between 0 MPa and 25 MPa, the effective contact pressure and the maximum plastic strain of the B-ring cylinder side and the end-cover side are almost the same. However, at 15 MPa, plastic deformation of the B ring occurs, and the contact width increases suddenly, resulting in a sudden decrease in  $Q$ . Average contact pressure and maximum plastic strain are greater on the cylinder side than the end-cover side when the pressure is between 25–75 MPa, which is due to the higher temperature of the cylinder in this stage, as shown in Figure 10c. This causes the thermal expansion of the cylinder to be larger than that of the end cover, and the contact surface of the cylinder shifts inward due to the displacement constraint of the clamp; therefore, the effective contact pressure and the maximum plastic strain of the B-ring cylinder side are higher than those of the end-cover side at this stage. When the medium pressure in the reactor is between 75 MPa and 160 MPa, the average contact pressure and the maximum plastic strain on the end-cover side of the B ring are generally higher than those on the cylinder side, which is due to the end cover rotating counterclockwise under the action of medium pressure around the contact point between the clamp and the end cover, as shown in Figure 12, resulting in increased contact pressure with the B-ring and higher maximum plastic strain.

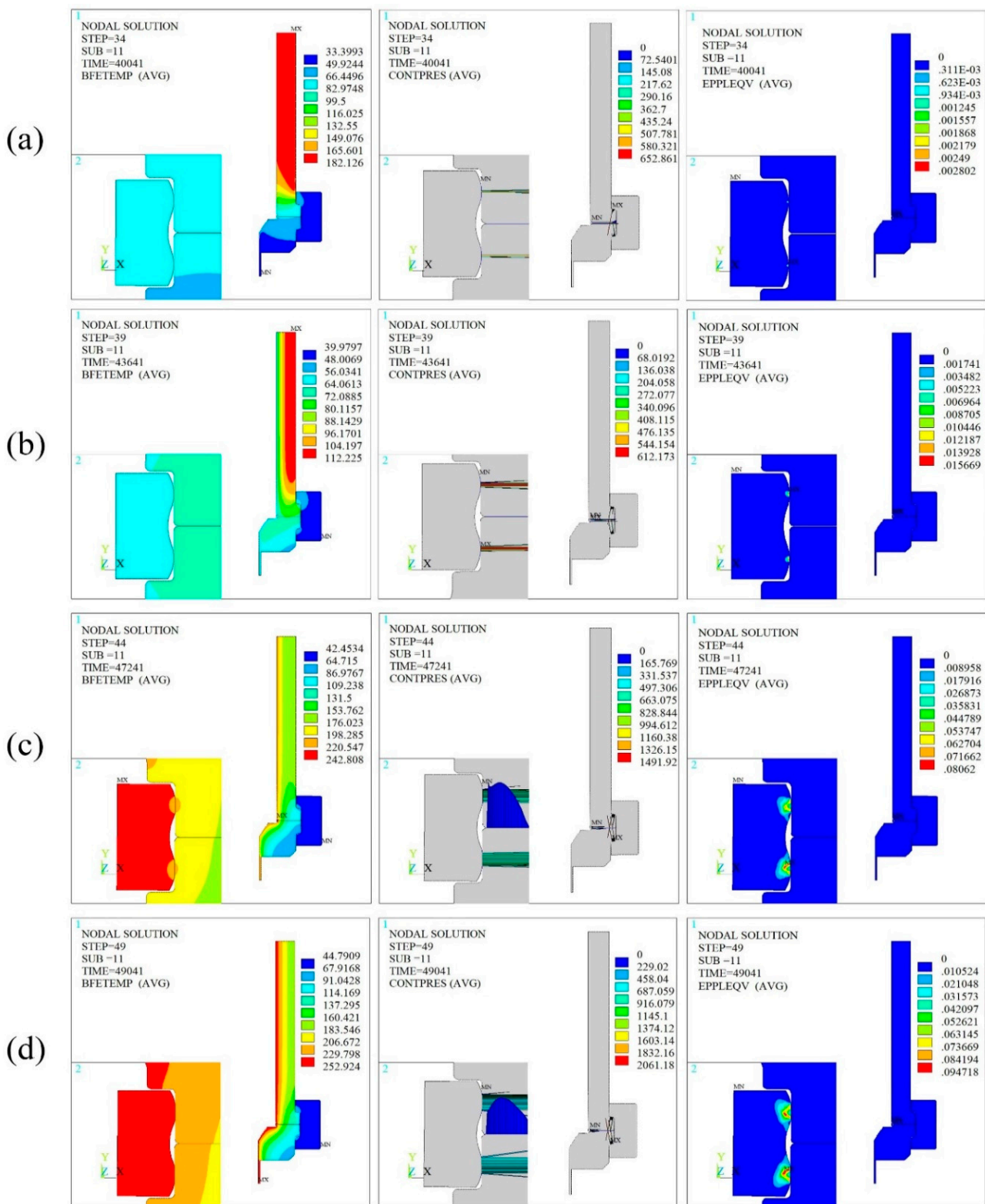
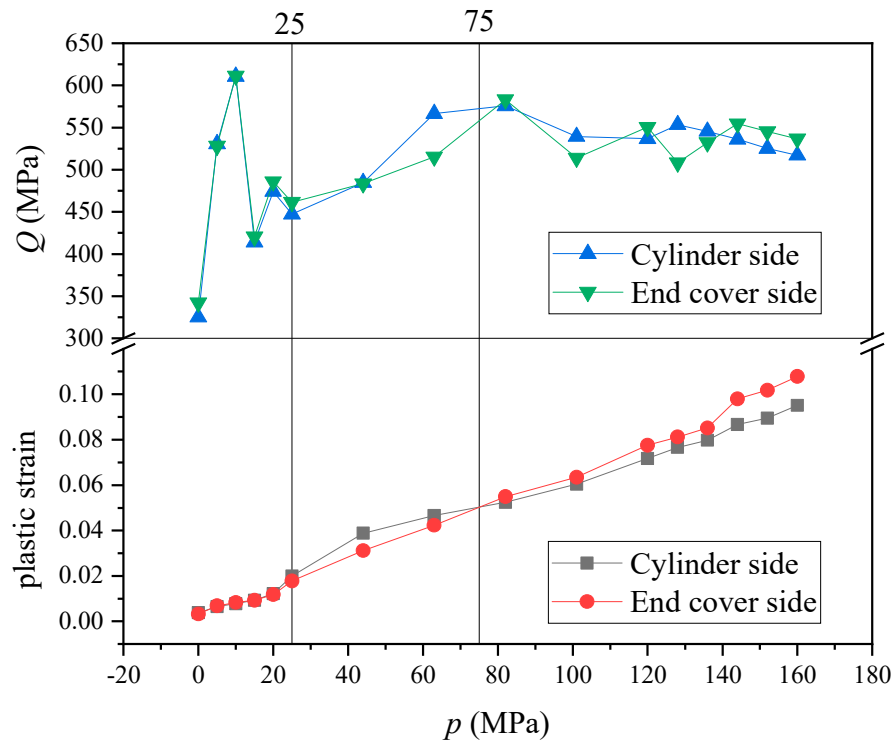
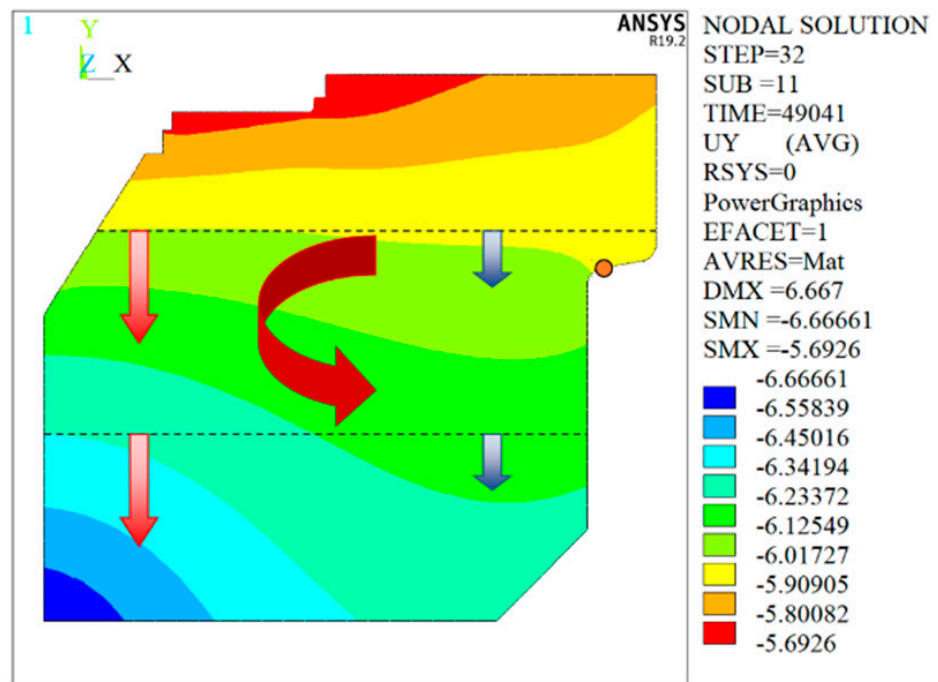


Figure 10. Finite element calculation results of the heating and pressurization process. (a) 0 MPa–150 °C; (b) 25 MPa–60 °C; (c) 120 MPa–215 °C; (d) 160 MPa–251 °C.



**Figure 11.** Changes in the average contact pressure and plastic deformation in the process of heating and pressurization.



**Figure 12.** Y-direction displacement contour of the end cover.

### 5.2.3. Calculation Results of the Process of Cooling and Depressurizing

The temperature contours, the contact pressure contours of the B ring and the plastic deformation contours at different times during the cooling and depressurizing stage of the reactor are shown in Figure 13, and the change in effective contact pressure of the B ring with medium pressure is shown in Figure 14. Within the medium-pressure range of 160–30 MPa, the contact pressure changes on the end cover side and the cylinder side are

basically the same. However, in the process of reducing the medium pressure from 30 MPa to 0 MPa, the effective contact pressure on the end cover side fluctuates violently, reaching 0 MPa when the pressure is reduced to 10 MPa. This is due to the deflected end cover slowly rotating with the decrease in medium pressure and the seal being closer to line contact. Due to excessive plastic deformation on the side of the B-ring end cover, the contact pressure of B-ring end cover is low or even 0 under low pressure, and leakage occurs.

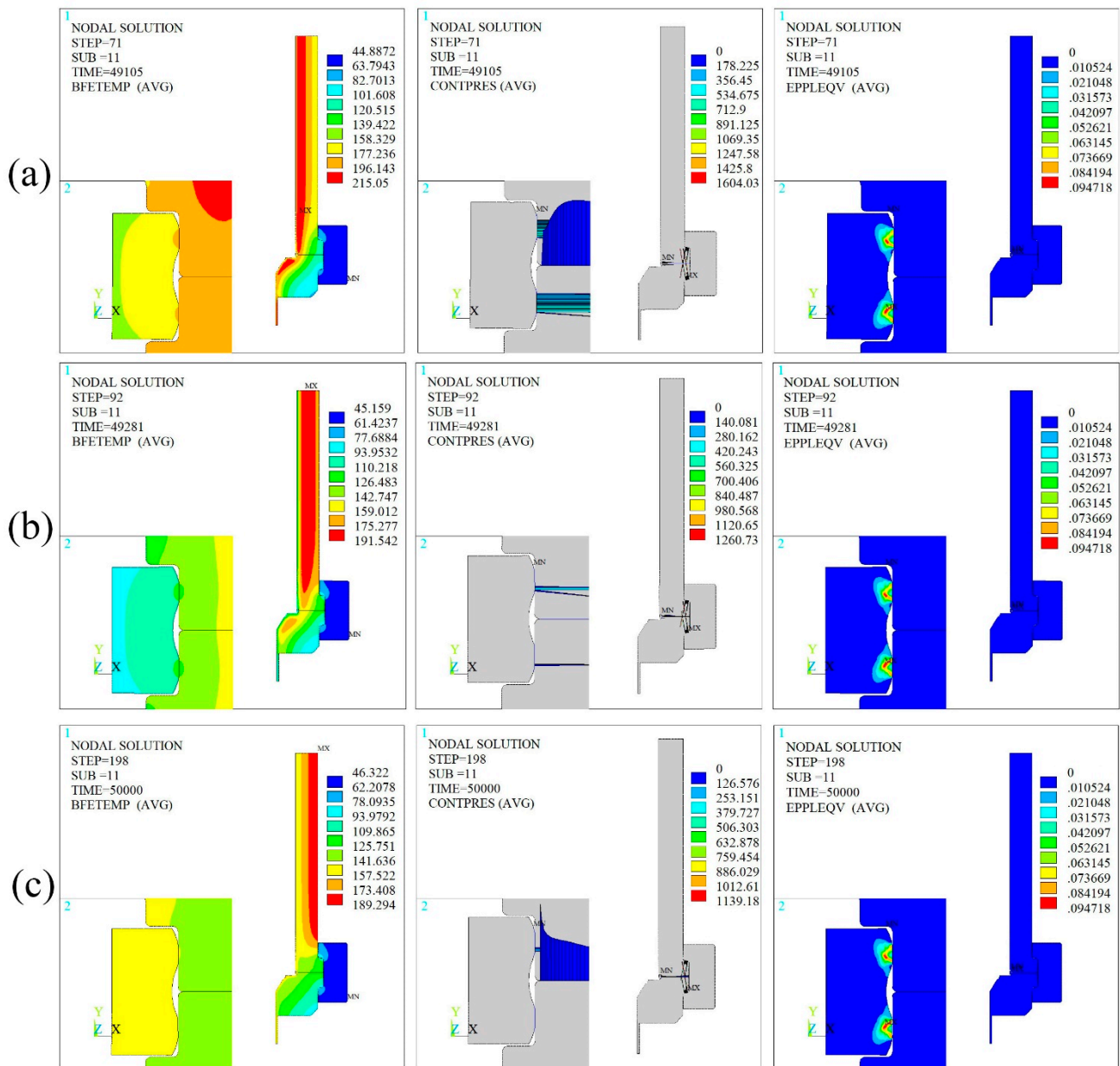


**Figure 13.** Calculation results of the cooling and depressurizing process. (a) 110 MPa–65 °C; (b) 16 MPa–95 °C; (c) 0 MPa–150 °C.

#### 5.2.4. Leakage Analysis

The contact pressure of each node on the contact surface of the B-ring cylinder side and end-cover side were extracted under different medium pressures in the process of heating and pressurization or cooling and depressurizing to calculate the average values, which were the average contact pressure,  $Q$ , of the B-ring contact surface in each case. Then,



the sealing rates were calculated as defined in Section 3. The variations of sealing rate of B-rings made of 10, 20 and 16 Mn steels with medium pressure are shown in Figure 15.

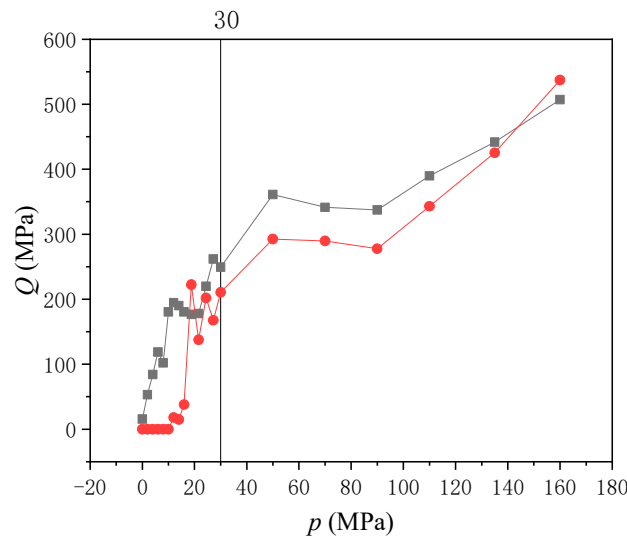


Figure 14. Change curve of effective contact pressure during cooling and depressurization.

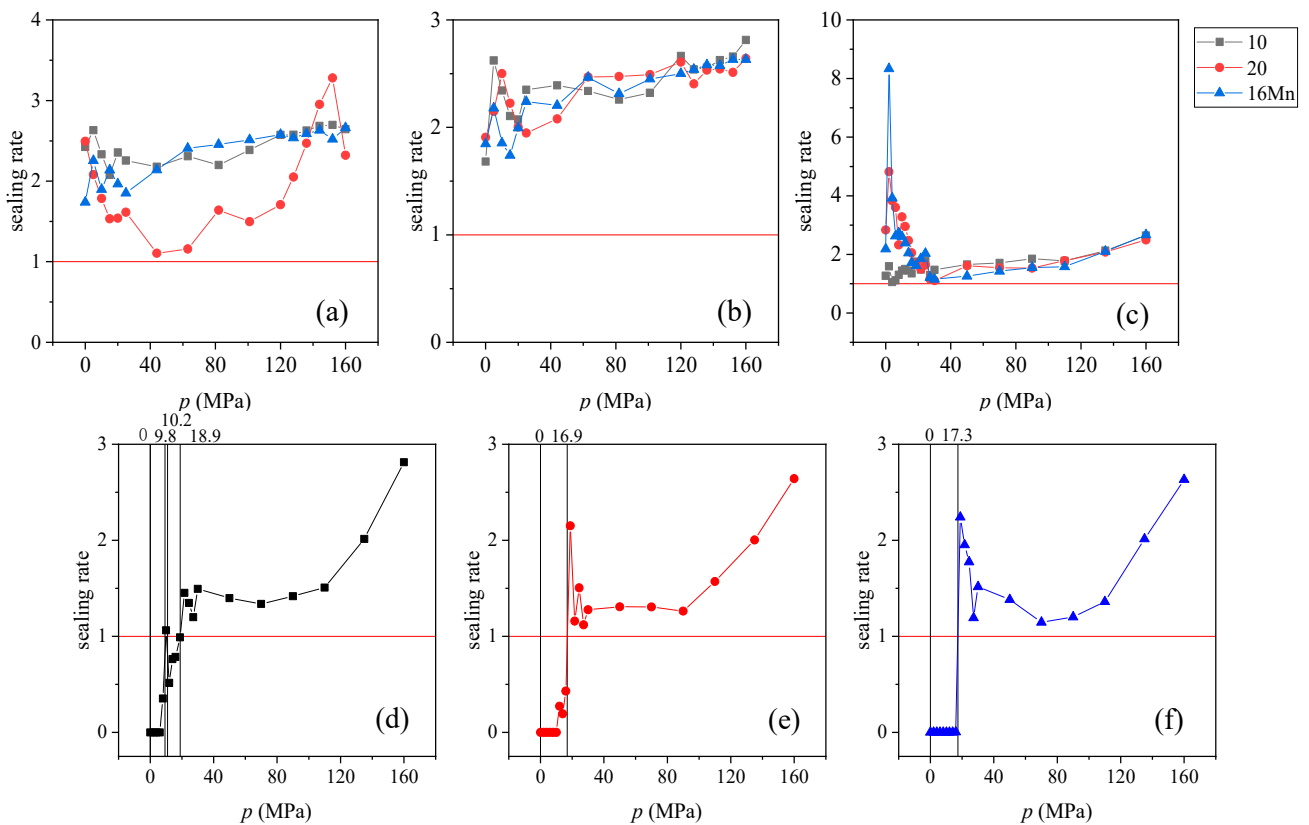


Figure 15. Medium pressure sealing rate curves. (a) Heating and pressurization (cylinder side); (b) heating and pressurization (end-cover side); (c) cooling and depressurization (cylinder side); (d–f) cooling and depressurization (end-cover side).

As shown in Figure 15, when the medium pressure on end-cover side of 10, 20 and 16 Mn steel B rings is in the range of 18.9–10.2 MPa, 9.8–0 MPa, 16.9–0 MPa and 7.3–0 MPa, the sealing rates are less than 1, i.e., within leakage pressure range. The leakage of the 10 steel B ring is divided into two intervals because steam is introduced into the jacket when the pressure is reduced to 16 MPa, and the reactor is heated up, which increases the contact

pressure between the B ring and the end cover, as shown in Figure 2. Then, the leakage time,  $t$  of, these leakage intervals was determined according to the temperature–pressure curve shown in Figure 2. The leakage parameter is defined as the product of the average leakage pressure of each leakage interval and the leakage time, i.e.,  $\Phi = \sum (\bar{p} \times t)$ . Therefore, the leakage parameters under this calculation condition are 102.50 MPa·min, 102.13 MPa·min and 104.27 MPa·min.

### 5.3. Analysis and Discussion on Influencing Factors of Sealing Performance

The analysis and calculation presented in Section 4.2.4 show that the contact pressure of the sealing surface is considerably affected by the arc radius,  $R_1$ ; interference,  $\delta$ ; and material properties of the B ring. Therefore, the influence of interference,  $\delta$ , and material properties on the sealing performance were discussed; then, the influence of the B-ring arc radius on the sealing performance was further studied under optimal interference, and on this basis, the optimal value was determined.

#### 5.3.1. Influence of Interference ( $\delta$ ) and B-ring Material on Sealing Performance

Under the same size of B ring, the influence of interference and material on effective contact pressure,  $Q$ , and contact width,  $a$ , were discussed and calculated according to the parameters listed in Table 5.

**Table 5.** Calculation scheme of interference ( $\delta$ ) and material <sup>1</sup>.

$\delta$ /mm \backslash Material	10	20	16 Mn	NiCrMoV	4140
0.05	LS11	LS12	LS13	LS14	LS15
0.15	LS21	LS22	LS23	LS24	LS25
0.25	LS31	LS32	LS33	LS34	LS35
0.35	LS41	LS42	LS43	LS44	LS45

<sup>1</sup> The circular radius  $R_1$  of the B ring in the table is 14.3 mm.

The B-ring seal structures specified in Table 5 were simulated and calculated. According to the calculation results of the cooling and depressurizing stage, the leakage pressure range, leakage duration and leakage parameters were sorted according to method described in Section 5.2.4. The results are shown in Table 6, and the variation of leakage parameters with material yield stress and interference of the B ring is shown in Figure 16. In the calculation range, B rings made of materials with a higher yield stress (NiCrMoV, 4140) do not leak, whereas B rings made of materials with a lower yield stress (10, 20 and 16 Mn) leak to varying degrees. This is because the plastic deformation of the end-cover side of B rings made of materials with low yield stress is relatively large during heating and pressurization (the plastic strain contour is shown in Figure 17a). When the reactor is cooled and depressurized to the lower pressure, the contact pressure between the B ring and the sealing surface is too low, resulting in leakage of the reactor.

**Table 6.** Leakage parameters of B rings of various materials under different interference values.

Serial Number	Leak Pressure /MPa		Leak Duration /min	Leak Parameter /MPa·min
LS11	19.27	15.16	0.88	36.93
	7.62	0	5.73	
LS21	18.87	10.23	4.56	102.50
	9.82	0	7.38	
LS31	18.76	0	12.19	114.40
LS41	19.69	16.08	0.25	34.17
	8.90	0	6.66	

Table 6. Cont.

Serial Number	Leak Pressure /MPa		Leak Duration /min	Leak Parameter /MPa·min
LS12	17.93	0	12.14	108.81
LS22	16.93	0	12.07	102.13
LS32	16.39	0	12.03	98.54
LS42	16.5	0	12.04	99.30
LS13	19.85	0	12.27	121.83
LS23	17.25	0	12.09	104.27
LS33	16.62	0	12.04	100.09
LS43	16.76	0	12.05	101.04
LS14	0	0	0	0
LS24	0	0	0	0
LS34	0	0	0	0
LS44	0	0	0	0
LS15	0	0	0	0
LS25	0	0	0	0
LS35	0	0	0	0
LS45	0	0	0	0

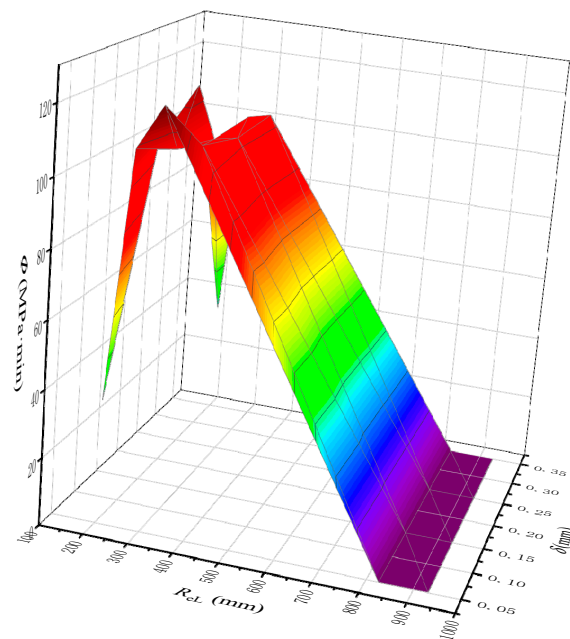


Figure 16. Variation trend of leakage parameters.

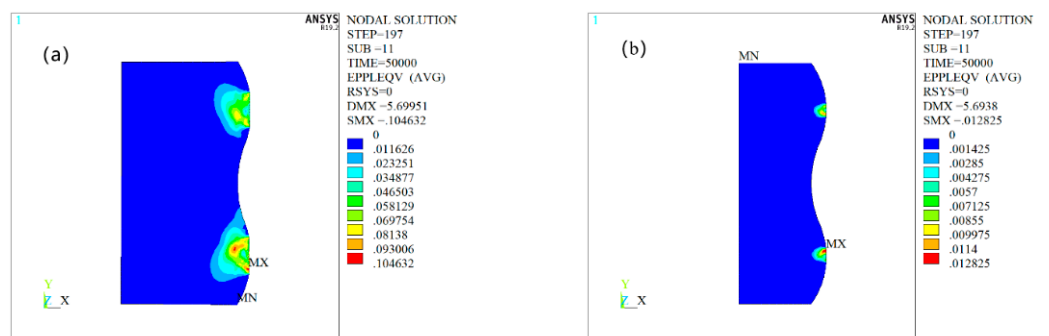
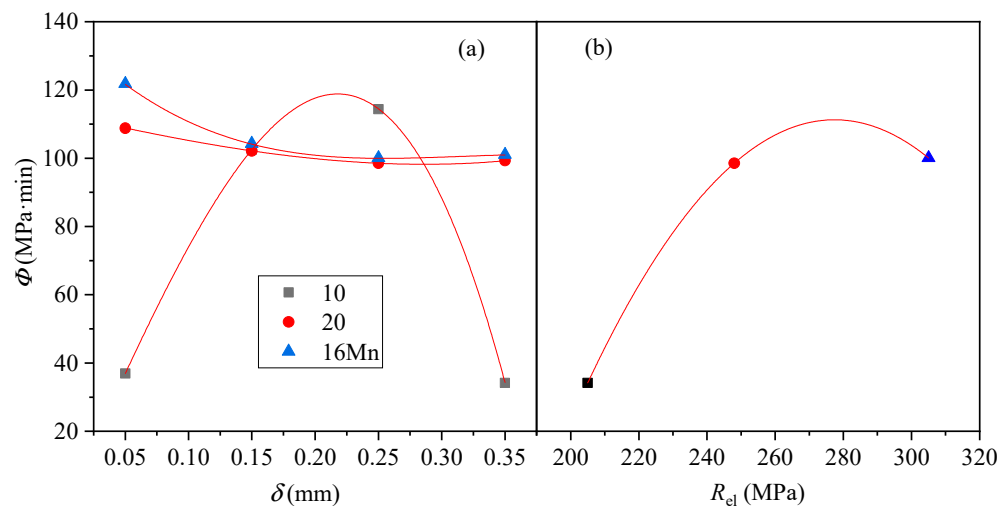


Figure 17. Plastic strain contour of B-rings made of 10 and 4140 steel. (a) 10steel; (b) 4140 steel.

The change in leakage parameters of the B rings for 10, 20 and 16 Mn steels are shown in Figure 18a. For a 10 Mn steel B ring in the range of 0.05–0.35 mm interference, the leakage parameter first increases and then decreases. When the interference is 0.22 mm, the leakage parameter reaches a maximum of 118.7 MPa·min, and the minimum leakage parameter is 34.17 MPa·min when the interference is 0.35 mm. However, the leakage parameters of B rings made of 20 and 16 Mn steel gradually decrease and tend to be stable in the range of 0.05–0.35 mm interference.



**Figure 18.** Leakage parameters of B rings of different materials are influenced by interference and yield stress. (a) Influence of interference on the leakage parameters of B rings made of different materials; (b) influence of yield stress on leakage parameters.

The radial displacement of the contact position between the outer side of the B ring and the sealing surface of the end cover of the three materials changes with the interference is shown in Figure 19a. Larger interference results in smaller radial displacement, which means a larger gap with the sealing surface and worse sealing performance. In addition, due to the low yield stress of these three materials, the B ring will produce plastic deformation during the process of increasing temperature and pressure, as shown in Figure 19b; the higher the interference, the lower the plastic strain. With 20 and 16 Mn steel, compressive plastic strain will occur. Obviously, higher expanded plastic strain is beneficial in that it reduces the gap between the B ring and the sealing surface after cooling and depressurization. Higher expanded plastic strain leads to better the sealing. Conversely, compressed plastic strain is not good for sealing.

Considering the plastic strain at the inner diameter position of the B ring and the radial displacement at the outer diameter position, the change in clearance between the outer side of the B ring and the sealing surface of the end-cover side with interference is shown in Figure 19c. The variation trend is consistent with that of the leakage parameters given in Figure 18a.

The variation trend of the minimum leakage parameters of three B-ring materials with yield stress is shown in Figure 18b. The minimum leakage parameter varies parabolically. When the yield stress is 277 MPa, the leakage parameter reaches its maximum value. Among the three materials with smaller yield stress, the leakage parameter of the B ring made of 10 steel is the smallest.

For a B ring with high yield stress (NiCrMoV, 4140), although there is no leakage within the calculation range, plastic deformation of the contact position appears successively at the B-ring, the sealing surface of the reactor cylinder and the end cover. The plastic strain increases with the interference and the yield stress of the B-ring material (as shown in Figure 20).

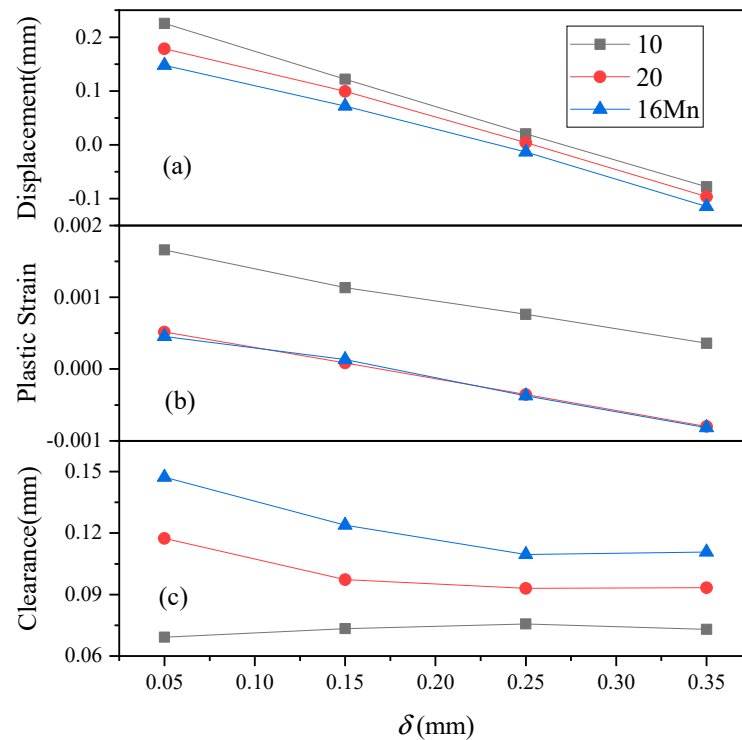


**Figure 19.** Deformation trend diagram of the B ring on the end-cover side. (a) Node displacement of outside diameter B ring; (b) circumferential strain of inner diameter of B ring; (c) clearance between B ring and end cover after depressurization.

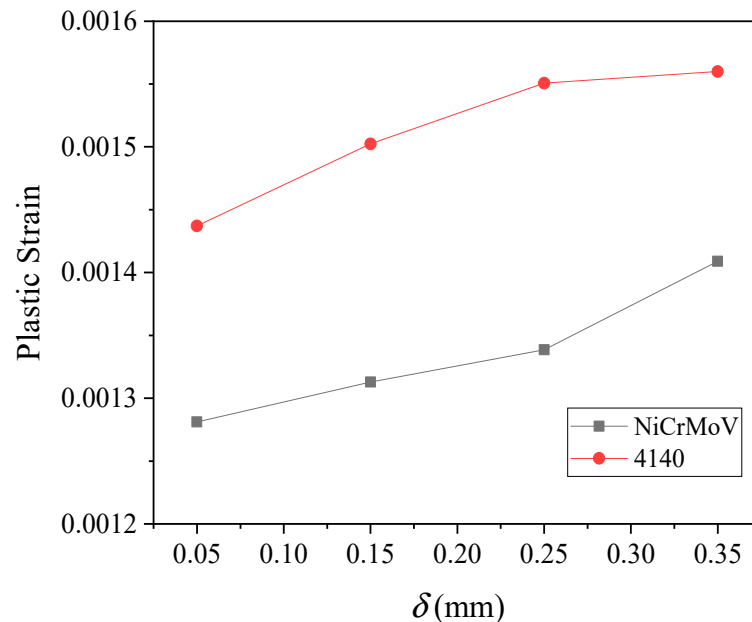


**Figure 20.** Circumferential plastic strain of the sealing surface on the cylinder side of the reactor.

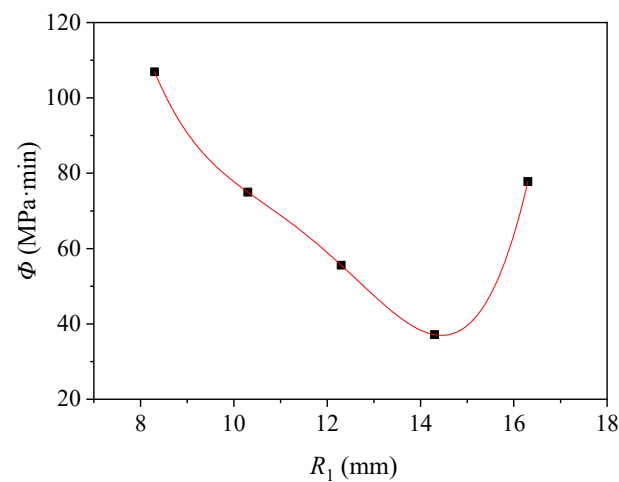
### 5.3.2. Influence of Arc Radius ( $R_1$ ) on Sealing Performance of the B Ring

Taking 4140 and 10 steels as examples, the influence of arc radius,  $R_1$ , on sealing performance was explored. The calculation scheme is shown in Table 7. The interference of the two materials with good sealing performance was used for calculation, which was 0.15 mm for 4140 steel and 0.05 mm for 10 steel.

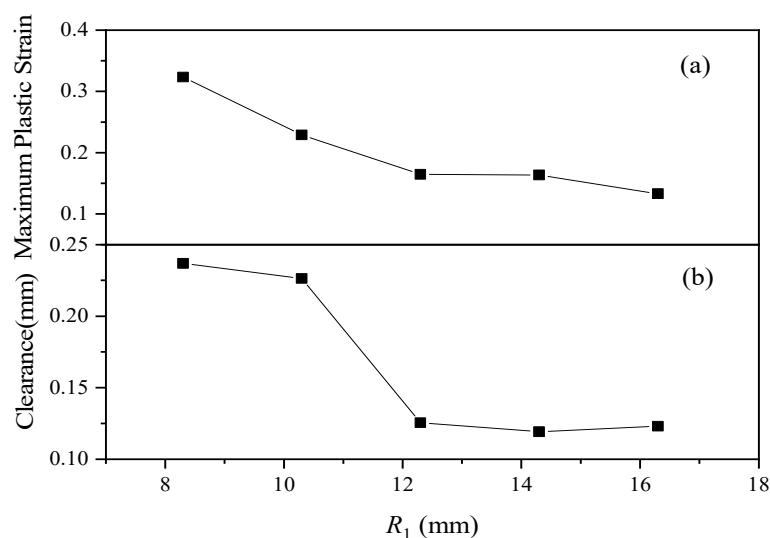
**Table 7.** Calculation scheme of arc radius ( $R_1$ ) and material type.

$R_1$ /mm	Material	10	4140
8.3		LD11	LD12
10.3		LD21	LD22
12.3		LD31	LD32
14.3		LD41	LD42
16.3		LD51	LD52

The B-ring seal structures specified in Table 7 were simulated and calculated. Based on the calculation results of the cooling and decompression stage, the leakage parameters are sorted according to the method introduced in Section 5.2.4. The leakage parameters of the B rings made of 10 and 4140 with different arc radii are shown in Figure 21. Leakage occurs with each arc radius value for 10 steel, but 4140 steel does not leak at all.

**Figure 21.** Influence of  $R_1$  on leakage parameters of a B ring made of 10 steel.

The leakage parameter of a B ring made of 10 steel first decreases and then increases with an increase in arc radius,  $R_1$ . On the one hand, with a smaller arc radius ( $R_1$ ) and contact width of the B-ring, higher plastic strain is generated in the heating and boosting stage, as well as the production stage, as shown in Figure 22a.

**Figure 22.** Influence of  $R_1$  on maximum plastic strain and clearance of the B ring. (a) Maximum plastic strain; (b) clearance.

When the reactor is cooled and depressurized to a lower pressure, there is not enough spring back, and the reactor will leak. On the other hand, when the arc radius,  $R_1$ , is larger, the  $h'$  is smaller, and the overall thickness of the B ring decreases. At this time, the B ring is more prone to radial deformation under the same pressure and temperature load. However, because of the larger contact width, the plastic strain is lower, as shown in Figure 22a, and the maximum plastic deformation increases, resulting in a higher minimum clearance between the end cover and the B ring and increased leakage parameters, as shown in Figure 22b. The combined effect of the two aspects makes the leakage parameter the smallest when  $R_1 = 14.3$  mm; the sealing performance of the B-ring with this  $R_1$  is the best.

Although a B ring of made of 4140 steel will not leak, the plastic strain of the contact surface of the end cover first decreases and then increases with an increase in the arc radius ( $R_1$ ), reaching its minimum value at  $R_1 = 14.3$  mm, as shown in Figure 23. This is because, on the one hand, the larger the radius,  $R_1$ , of the circular arc of the B ring and the contact width cause a lower the contact pressure under the same pressure and temperature load, which leads to lower plastic deformation of the end cover. On the other hand, the  $h'$  decreases with decreased arc radius ( $R_1$ ), and the overall thickness of the B ring decreases accordingly. Under the same pressure and temperature load, the B ring is more prone to radial deformation, resulting in a larger contact surface load, so the plastic deformation of the end cover increases, especially when the arc radius,  $R_1$ , is increased from 14.3 mm to 16.3 mm. As a result, the structure with this  $R_1$  has the best sealing effect.

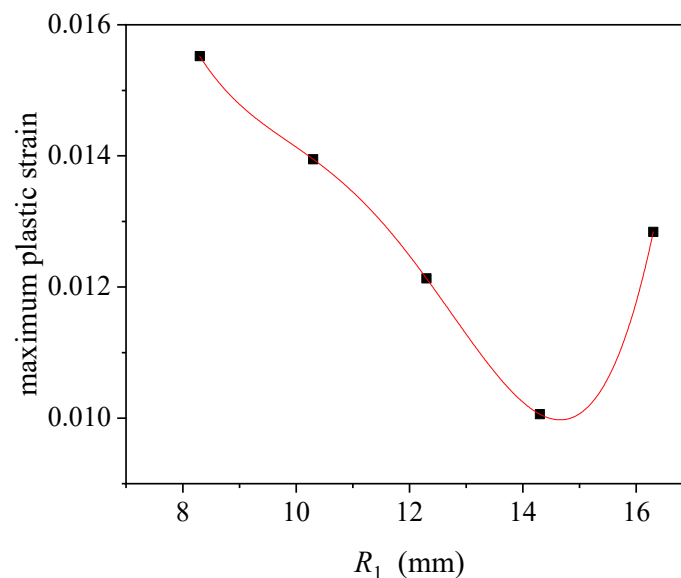


**Figure 23.** Maximum plastic strain of end-cover contact surface.

#### 5.4. Comparison of Results between Theoretical Calculation and Finite Element Analysis in Elastic Range

For a B ring made of 4140 steel with an arc radius,  $R_1$ , of 14.3 mm at a 0 min working point, contact pressure of finite element analysis value ( $Q^F$ ) and theoretical calculation value ( $Q^A$ ), contact width of finite element analysis value ( $a^F$ ) and theoretical calculation value ( $a^A$ ), total contact load ( $N = Q \cdot a$ ) of finite element analysis value ( $N^F$ ) and theoretical calculation value ( $N^A$ ), as well as their relative errors ( $E^Q$ ,  $E^a$  and  $E^N$ ) are shown in Table 8 with varying interference,  $\delta$ . The contact pressure, contact width, total contact load and relative error of a 4140 steel B ring at the 0 min operating point when the interference,  $\delta$ , is 1.5 mm are shown in Table 9.

As shown in Tables 8 and 9, the relative errors between the analytical calculation values of effective contact pressure and contact width and the finite element analysis values are less than 25%, and those of total contact load are less than 15%, which shows that the two results are basically consistent.

In addition, as shown in Figure 24, the radial displacements of the B ring and the sealing surface position of the cylinder obtained by analytical analysis and finite element analysis are basically consistent at the assembly condition, 0 min and 60 min operating points, and their relative errors are less than 20%.

**Table 8.** Comparison between finite element solution and analytical solution with varying interference.

$\delta$ /(mm)	$Q^F$ /(MPa)	$Q^A$ /(MPa)	$E^Q$	$a^F$ /(mm)	$a^A$ /(mm)	$E^a$	$N^F$ /(N)	$N^A$ /(N)	$E^N$
0.05	224.34	275.49	0.23	0.25	0.19	-0.24	57.08	52.12	-0.09
0.15	499.70	421.51	-0.16	0.26	0.29	0.11	129.35	122.01	-0.06
0.25	591.14	528.47	-0.11	0.34	0.36	0.07	200.12	191.80	-0.04
0.35	541.45	617.03	0.14	0.51	0.42	-0.17	273.73	261.46	-0.04

**Table 9.** Comparison between finite element solution and analytical solution with varying arc radius.

$R_1$ /(mm)	$Q^F$ /(MPa)	$Q^A$ /(MPa)	$E^Q$	$a^F$ /(mm)	$a^A$ /(mm)	$E^a$	$N^F$ /(N)	$N^A$ /(N)	$E^N$
8.3	539.77	538.55	0.00	0.23	0.21	-0.07	124.65	115.61	-0.07
10.3	508.06	489.17	-0.04	0.24	0.24	0.01	122.08	118.36	-0.03
12.3	502.32	451.51	-0.10	0.25	0.27	0.07	125.37	120.42	-0.04
14.3	499.70	421.51	-0.16	0.26	0.29	0.11	129.35	122.01	-0.06
16.3	478.94	396.86	-0.17	0.30	0.31	0.04	143.68	123.29	-0.14

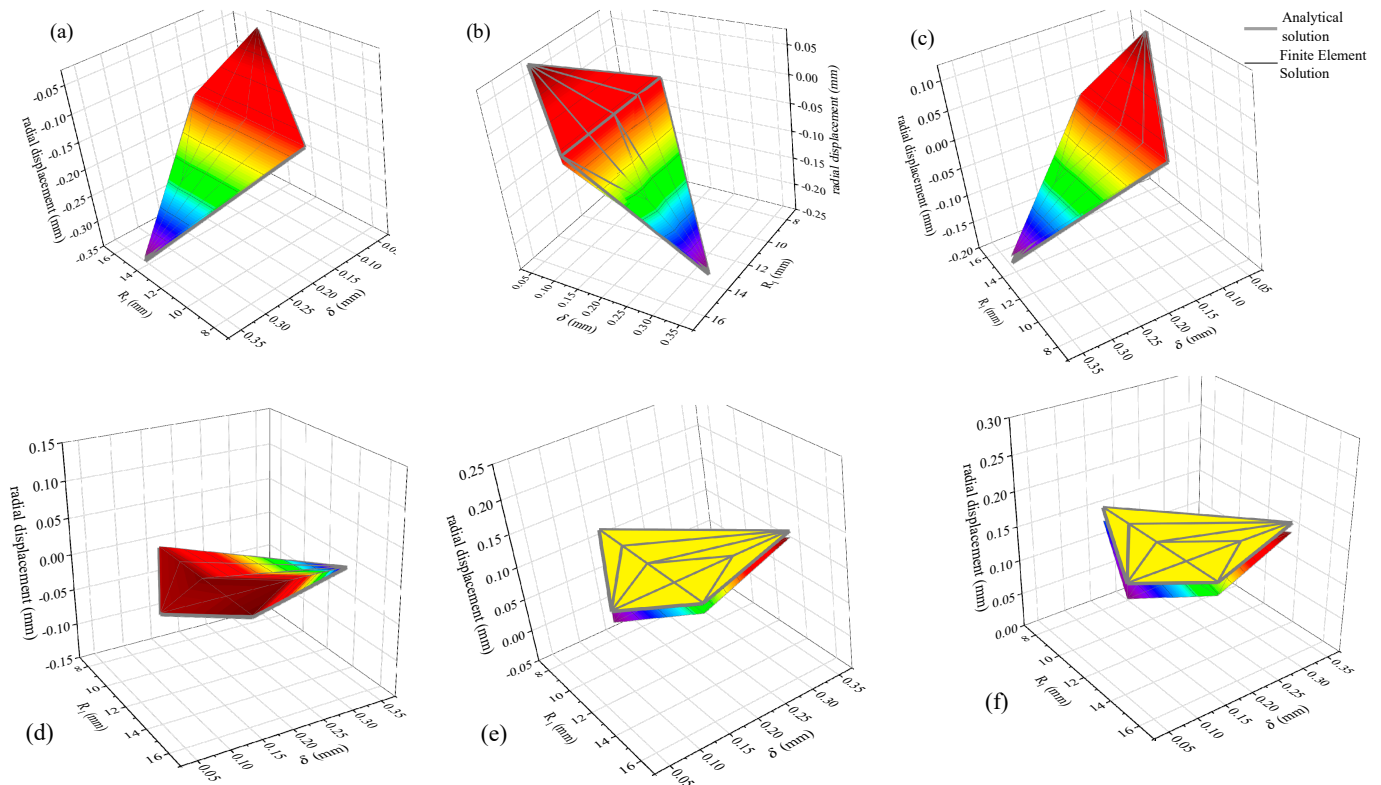


**Figure 24.** Comparison between the analytical solution and the finite element solution of the radial displacement of the contact surface between the B ring and the cylinder. (a,d) Assembly condition; (b,e) 0 min; (c,f) 60 min; (a-c) B-ring radial displacement; (d-f) radial displacement of cylinder contact surface.

The main reasons for the errors between analytical solution and finite element solution are as follows: (1) The contact force between the B ring and the sealing surface is applied at



the two peak positions, but Equation (22) is an approximate derivation based on a uniform load. (2) The radial displacement caused by contact pressure on the sealing surface of the cylinder is calculated approximately according to the internal pressure. Because the analytical solution and the finite element solution are basically the same in the elastic range, it can be considered that the analytical solution in Section 4.2.4 has a certain reference value for the analysis of the B-ring sealing performance.

## 6. Conclusions

Based on the elastic deformation analysis, the deformation co-ordination equation of a B-ring sealing structure of a high-pressure reactor under the action of temperature and pressure was established, and a contact pressure calculation formula of the sealing structure was obtained. A finite element analysis model of the sealing structure was established; transient temperature field analysis was carried out for startup and shutdown; and contact analysis was carried out for the interference assembly, as well as startup and shutdown conditions. Based on the evaluation criteria of sealing performance with the proposed sealing rate and leakage parameters, the effects of material properties, interference, B ring size, etc. on the B-ring sealing performance of a high-pressure reactor were investigated. Our analyses yielded the following results.

(1) During heating and pressurization, a B ring made of 10, 20, 16 Mn, NiCrMoV or 4140 steel will not leak in the range of the discussed interference and the wave radius of the B ring. During cooling and depressurization, only a B ring with high yield stress will not leak, such as those made of NiCrMoV and 4140.

(2) Although a B-ring made of NiCrMoV or 4140 steel with high yield stress will not leak, the B-ring, the sealing surface of the cylinder and the end cover will yield plastic deformation during heating and pressurization. When replacing a B-ring, it is necessary to adjust its size according to the plastic deformation of the sealing surface to ensure that the interference requirement is satisfied.

(3) For B rings made of 10, 20 or 16 Mn steels with lower yield stress, due to the plastic deformation caused by the interference assembly, as well as heating and pressurization, a radial gap is generated between the outer side of the B ring and the sealing surface at the end cover, resulting in sealing failure. However, leakage parameters can be minimized by lower interference and a moderate wave radius.

(4) Compared with the results of finite element analysis, the contact pressure of the B ring based on elastic deformation analysis is higher, and the contact width is smaller, but the contact load is almost the same. Elastic deformation analysis is helpful to some extent for sealing performance analysis of the B-ring seal structure.

### Highlight

The deformation coordination equation of the B-ring seal structure of high-pressure reactor under the action of temperature and pressure is established, and the formula of contact pressure gauge at the sealing part is obtained.

Sealing performance is analyzed by finite element method for the B shape ring sealing structure. And the effects of material properties, interference, and wave radius of the B shape ring on the sealing performance are discussed.

**Author Contributions:** Numerical simulations: H.G. and C.W.; methodology: H.G. and B.G.; conceptualization: J.D. and B.G.; writing—original draft preparation: H.G.; writing—review and editing: J.D. and B.G.; project administration: C.W.; funding acquisition: Y.A. All authors have read and agreed to the published version of the manuscript.

**Funding:** This research was supported by the National Key Research and Development Program of China, No. 2018YFC0808600.

**Institutional Review Board Statement:** Not applicable.

**Informed Consent Statement:** Not applicable.

**Data Availability Statement:** Not applicable.

**Conflicts of Interest:** The authors declare no conflict of interest.

### Notation

$A$	Width of B ring, mm
$a$	Width of contact, mm
$c$	Specific heat capacity, J/(kg K)
$E$	Young's modulus, GPa
$h$	Minimum thickness of B ring, mm
$h'$	Height of wave of B ring, mm
$\bar{h}$	Average thickness of B ring, mm
$K$	Diameter ratio of nozzle
$l$	Center distance of B ring, mm
$m$	Gasket factor
$p$	Medium pressure, MPa
$p_i$	Contact pressure of nodal, MPa
$Q$	Average contact pressure, MPa
$R_{eL}$	Yield stress, MPa
$R_1$	Inner arc radius of B ring, mm
$R_2$	Outer arc radius of B ring, mm
$r_{B1}$	Inside radius of B ring, mm
$r_{B2}$	Equivalent outer radius of B ring, mm
$r_{c1}$	Radius of sealing surface, mm
$r_{c2}$	Outer radius of clamp, mm
$r_c$	Inner arc radius of cylinder, mm
$T$	Temperature, °C
$y$	Node ordinate, mm
$\alpha$	Coefficient of thermal expansion, $\times 10^{-6} \text{ m}/^\circ\text{C}$
$\delta$	Initial interference, mm
$\lambda$	Thermal conductivity, W/(m·K)
$\mu$	Poisson ratio
$\sigma$	Stress, MPa
$\Phi$	Leakage parameters, MPa min
$\Delta_B^P, \Delta_B^T, \Delta_B^Q$	Radial displacement of B ring, mm
$\Delta_{c1}^P, \Delta_{c1}^T, \Delta_{c1}^Q, \Delta_{c1}^{P+Q}$	Radial displacement of cylinder, mm

### References

1. Yamauchi, T.; Manabe, Y.; Nishimoto, T. Self-Tightening Type Sealing Device. US20050077686A1, 14 April 2005.
2. Yang, X.L.; Yang, Z.G.; Ding, Q. Failure analysis of O-ring gaskets of the electric hydraulic system in the nuclear power plant. *Eng. Fail. Anal.* **2017**, *79*, 232–244. [[CrossRef](#)]
3. Trojnacki, A. Druckstandfestigkeit und Betriebseigenschaften von Doppelwellendichtungen. *Chem. Ing. Tech.* **2011**, *83*, 377–385. [[CrossRef](#)]
4. Gao, B.; Liu, B.; Wang, C.; Yu, C.; Gao, H.; Wang, T.; Chen, X. Leakage analysis of B shape ring self-energized seal in high pressure polythene polymerizer due to the aging of its nonmetallic ring. *Int. J. Press. Vessel. Pip.* **2021**, *194*, 104549. [[CrossRef](#)]
5. Freeman, A.R. *Gaskets for High Pressure Vessels, Pressure Vessel and Piping Design, Collected Papers 1927–1959*; ASME: Little Falls, NJ, USA, 1960.
6. Cracow University of Technology. *Realization of Technical Documentation of the Reactor 41/42 V-7 for the Polyethylene Installation*; Report TPP-5; Cracow University of Technology: Cracow, Poland, 2000.
7. Hua, E.L. *High Pressure Fast Open Self Tight Seal Structures for Supercritical Extraction Devices*; PETRO-Chemical Equipment: Baton Rouge, LA, USA, 1997.
8. Reeves, D.; Ruffin, M. Pressure Energized Gasket (PEG) Behavior and Seating Stress. In Proceedings of the Asme Pressure Vessels & Piping Conference 2013, Paris, France, 14–18 July 2013.
9. Wang, X.; Wang, R.; Li, P. Research on hydraulic expansion process of manufacturing bimetallic cralined pipe with self-energizing seal. *Chin. J. Mech. Eng.* **2004**, *40*, 72–76. (In Chinese) [[CrossRef](#)]
10. Ryś, J. An analysis of high pressure connections with wave-ring gasket. In Proceedings of the XXI Symposium on Machine Design, Rome, Italy, 8–13 June 2003; pp. 183–188.
11. Ryś, J.; Trojnacki, A.; Betleja, T. Theoretical analysis of metal wave-ring gasket for high pressure joints. In Proceedings of the Xth Int. Conf. Seals and Sealing Technology in Machines and Devices, Dresden, Germany, 6–10 June 2004; pp. 54–62.
12. Szybiński, B.; Trojnacki, A. Experimental verification of stress-strain analysis of metal wavering gasket. *Mech. Rev.* **2011**, *7*, 50–57.

13. Ryś, J.; Szybiński, B.; Trojnacki, A. Computational model of metal high pressure wave-ring gasket. *Tech. Trans. Ser. Mech.* **2006**, *11*, 63–87.
14. Szybinski, B.; Trojnacki, A. Analytical and Numerical Solutions of Metal High pressure Wave-Ring Gasket and Comparison with Experimental Results. *Arch. Mech. Eng.* **2015**, *62*, 19–44. [[CrossRef](#)]
15. Trojnacki, A.; Krasiski, M.; Szybiski, B. Analityczne i numeryczne badania wybranych metalowych uszczeltek wysokociśnieniowych. *Mechanik* **2016**, *8*, 1004–1008. [[CrossRef](#)]
16. Trojnacki, A.; Krasiski, M.; Szybiski, B. Investigations of metal gaskets for high pressure joints. *J. Kones* **2016**, *23*, 397–404. [[CrossRef](#)]
17. Trojnacki, A.; Szybiński, B. Investigations of strength and leak tightness of wavering gasket. *Czas. Tech. Mech.* **2015**, *4*, 143–163. [[CrossRef](#)]
18. *ASME.BPVC.II.D.M-2021*; ASME Boiler and Pressure Vessel Code an International Code. American Society of Mechanical Engineers: New York, NY, USA, 2021.
19. *GB/T 150-2011*; Pressure Vessel. China Standard Press: Beijing, China, 2011. (In Chinese)
20. Luo, Z.; Fei, Y.T.; Miao, E.M. Study on Deformation of Hole Parts in Steady-State Non-Uniform Temperature Field. *J. Appl. Sci.* **2005**, *4*, 424–427.
21. Xu, K.; Su, J.X.; Zhou, Y.D. Gear line contact and point contact theory and finite element analysis. *Mech. Transm.* **2014**, *38*, 5.
22. Tao, W.Q. *Numerical Heat Transfer*, 2nd ed.; Xi'an Jiao Tong University Press: Xi'an, China, 2001. (In Chinese)